

Parallel Inhibitory and Excitatory Trigemino-Facial Feedback Circuitry for Reflexive Vibrissa Movement

Highlights

- Vibrissa contact leads to brainstem-mediated feedback signals to facial motoneurons
- Intrinsic (protraction) motoneurons receive prompt inhibitory and excitatory feedback
- Extrinsic (retraction) motoneurons receive excitatory feedback
- These disynaptic reflexes are a substrate for fast, top-down modulation of touch

Authors

Marie-Andrée Bellavance,
Jun Takatoh, Jinghao Lu,
Maxime Demers, David Kleinfeld,
Fan Wang, Martin Deschênes

Correspondence

dk@physics.ucsd.edu (D.K.),
fan.wang@duke.edu (F.W.),
martin.deschenes@crulrg.ulaval.ca (M.D.)

In Brief

Bellavance et al. have identified three parallel, disynaptic sensorimotor loops that control contact-induced reflexive motion of the vibrissae in rodents. These anatomically low-level reflex arcs can incorporate the current goals and attention-driven focus of the animal.



Parallel Inhibitory and Excitatory Trigemino-Facial Feedback Circuitry for Reflexive Vibrissa Movement

Marie-Andrée Bellavance,^{1,6} Jun Takatoh,^{2,6} Jinghao Lu,² Maxime Demers,¹ David Kleinfeld,^{3,4,5,*} Fan Wang,^{2,*} and Martin Deschênes^{1,7,*}

¹Department of Psychiatry and Neuroscience, Laval University, Québec City, QC G1J 2G3, Canada

²Department of Neurobiology, Duke University Medical Center, Durham, NC 27710, USA

³Department of Physics, University of California, San Diego, La Jolla, CA 92093, USA

⁴Section of Neurobiology, University of California, San Diego, La Jolla, CA 92093, USA

⁵Department of Electrical and Computer Engineering, University of California, San Diego, La Jolla, CA 92093, USA

⁶These authors contributed equally

⁷Lead Contact

*Correspondence: dk@physics.ucsd.edu (D.K.), fan.wang@duke.edu (F.W.), martin.deschenes@crulrg.ulaval.ca (M.D.)

<http://dx.doi.org/10.1016/j.neuron.2017.06.045>

SUMMARY

Animals employ active touch to optimize the acuity of their tactile sensors. Prior experimental results and models lead to the hypothesis that sensory inputs are used in a recurrent manner to tune the position of the sensors. A combination of electrophysiology, intersectional genetic viral labeling and manipulation, and classical tracing allowed us to identify second-order sensorimotor loops that control vibrissa movements by rodents. Facial motoneurons that drive intrinsic muscles to protract the vibrissae receive a short latency inhibitory input, followed by synaptic excitation, from neurons located in the oralis division of the trigeminal sensory complex. In contrast, motoneurons that retract the mystacial pad and indirectly retract the vibrissae receive only excitatory input from interpolaris cells that further project to the thalamus. Silencing this feedback alters retraction. The observed pull-push circuit at the lowest-level sensorimotor loop provides a mechanism for the rapid modulation of vibrissa touch during exploration of peri-personal space.

INTRODUCTION

The most basic unit of motor action is a reflex arc. A sensory organ is activated by a stimulus and drives a motoneuron that leads to a response in an effector cell, usually a muscle. Reflex arcs are typically located in the hindbrain or spinal cord and mediate fast responses through positive or negative feedback loops. While the reflex arc can be formed by a direct connection from a sensory afferent to a motoneuron, frequently reflex arcs include a second-order neuron, or interneuron, between the sensory and motor neuron. The second-order neuron may play two roles: first, as a gate to modulate the effectiveness of the reflex

arc and second, as a relay to convey information to the brain or other parts of the body.

Reflex arcs are fundamental to touch that is mediated by the vibrissa system of rodents. Rhythmic motion of the vibrissae is driven by a central oscillator that can operate independently of direct sensory feedback (Welker, 1964; Gao et al., 2003; Berg and Kleinfeld, 2003; Moore et al., 2013). The effect of vibrissa contact on whisking kinematics has been studied in freely moving and head-restrained rats (Sachdev et al., 2003; Mitchinson et al., 2007; Grant et al., 2009; Deutsch et al., 2012; Hires et al., 2013; Voigts et al., 2015). The results of these studies are not clearly consistent. Upon contact with an object, vibrissae on the side of contact may rapidly and transiently protract (Sachdev et al., 2003), retract (Mitchinson et al., 2007), or exhibit a pump-like motion of retraction followed by protraction, denoted as a touch-induced pump by Deutsch et al. (2012) (Figure 1A). As discussed by Sherman et al. (2013), neuro-reflexive motion can occur through parallel pathways in the brainstem (Figure 1B). Reflexive retraction may occur by transient inhibition of the intrinsic motoneurons and/or by excitation of motoneurons that drive the extrinsic retractor muscles, i.e., maxolabialis and nasolabialis. Reflexive protraction may occur by transient excitation of the intrinsic motoneurons and/or by excitation of motoneurons that drive the extrinsic protraction muscle nasolabialis profundus.

Independent of the details of the motion, the lack of direct projections from primary vibrissa afferents to facial motoneurons (Hattox et al., 2002; Takatoh et al., 2013) implies that sensory feedback involves second-order or higher-order neurons. In fact, experiments in brainstem slice indicate that sensorimotor feedback is mediated by a disynaptic pathway that lies in the hindbrain (Nguyen and Kleinfeld, 2005). This circuit involves premotor neurons located in the oralis (spinal trigeminal subnuclei oralis [SpVO]) and rostral interpolaris (spinal trigeminal subnuclei rostral interpolaris [SpVlr]) subnuclei of the spinal trigeminal complex (Pinganaud et al., 1999; Takatoh et al., 2013; Sreenivasan et al., 2015). Transsynaptic labeling further revealed a differential distribution of trigeminal premotor neurons. Those that innervate the intrinsic protractor motoneurons are principally located in subnucleus SpVO, while premotor neurons that drive the extrinsic retractor motoneurons in the mystacial pad are

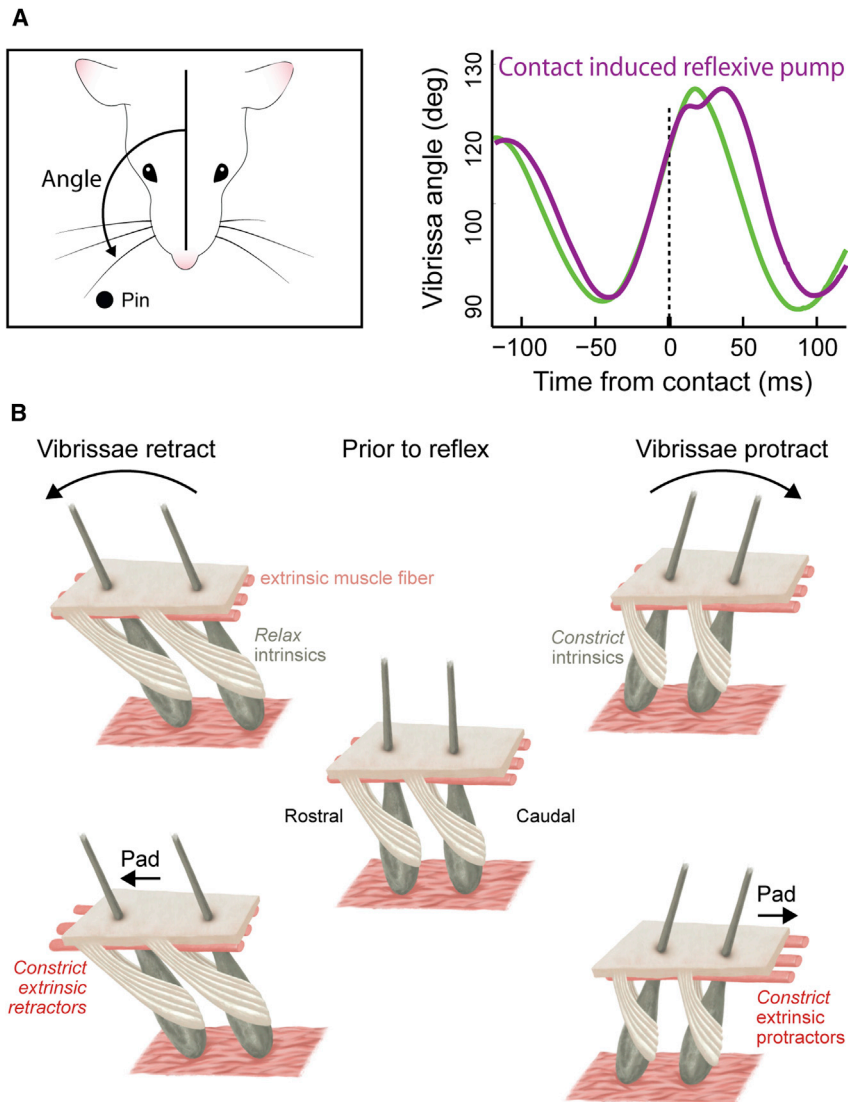


Figure 1. Basic Behavior and Vibrissae Mechanics

(A) Vibrissa contact leads to a pump-like motion, with a transient dip in the protraction of the vibrissae and an elongation of the interval of protraction. The left illustration shows the setup to observe contact while a head-fixed rat whisks, while the right image shows the angular dependence of the vibrissae during whisking in air versus touch to a pole. Data are from Deutsch et al. (2012).

(B) Cartoon of the muscles that control protraction and retraction of the vibrissa and may be involved in the reflex. Activation of the intrinsic muscles is the major drive of protraction. Activation of the extrinsic muscle nasolabialis profundus pulls the mystacial pad rostral and thus shifts the vibrissae toward protraction, while activation of the extrinsic muscles nasolabialis and maxillofacialis pulls the pad caudal and thus shifts the vibrissae toward retraction. The extrinsic muscle fibers (emfs) run underneath the skin between rows of vibrissae. Illustration by J. Kuhl.

preferentially clustered in subnucleus SpVlr (Takato et al., 2013; Sreenivasan et al., 2015). Thus, the known anatomy can support a mixed inhibitory and excitatory response (Deutsch et al., 2012; Sherman et al., 2013). Yet the specifics of this circuitry and the potential involvement of different muscle groups in the reflex arc (Figure 1B) remain an open issue.

Here we used intracellular recording, virus-based labeling methods, including intersectional genetic viral labeling, for tract tracing and neuronal activation and inactivation, as well as classical tracers, to decipher the circuitry involved in reflex control of facial motoneurons. We further extend past studies to include muscle nasolabialis profundus (Hill et al., 2008).

RESULTS

Anatomical Background

The facial nucleus is the sole output station that controls the activation of vibrissa muscles. It contains only alpha motoneu-

rons (Moore et al., 2015), no local circuit cells, and its motoneurons do not give off intranuclear axon collaterals (Friauf, 1986). Several studies have shown that the rodent facial musculature is anatomically mapped within the facial motor nuclear complex (Watson et al., 1982; Ashwell, 1982; Hinrichsen and Watson, 1984; Komiyama et al., 1984; Furutani et al., 2004; Klein and Rhoades, 1985; Takato et al., 2013; Sreenivasan et al., 2015; Deschênes et al., 2016). Motoneurons that innervate the intrinsic vibrissa muscles are located in the ventral lateral part of the nucleus, the extrinsic retractor muscles nasolabialis and maxillofacialis are represented dorsolaterally, and the extrinsic protractor muscle nasolabialis profundus is represented at the lateral most edge of the nucleus.

As a means to map premotor input to the extrinsic protractor muscle, Δ G-Rabies (Wickersham et al., 2007) was injected into muscle nasolabialis profundus (five juvenile mice). We observed retrograde labeling at the extreme lateral edge of the facial nucleus, transsynaptic labeling in the parafacial region and in the preBöttinger complex, but virtually no transsynaptic labeling in trigeminal sensory nuclei (three cells in five mice; Figure 2). We conclude that nasolabialis profundus motoneurons are not likely involved in short-latency reflex motion to whisker contact.

Response of Facial Motoneurons to Vibrissa Deflection in Anesthetized Rats

In a second series of experiments (eight rats), we examined synaptic events evoked in facial motoneurons by passive deflection of the vibrissae (Figure 3). Motoneurons were identified as intrinsic motoneurons on the basis of single-vibrissa protractions

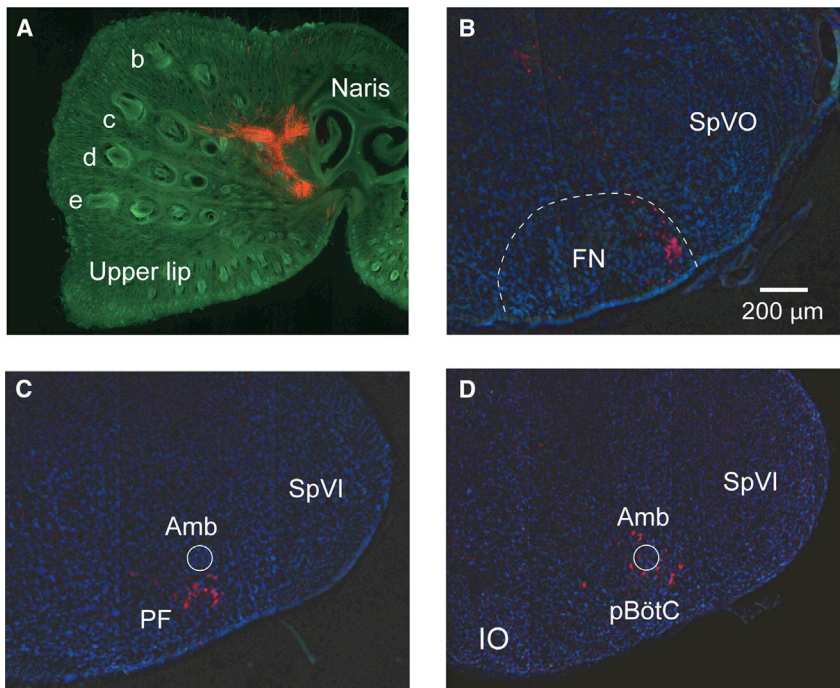


Figure 2. Absence of Innervation of Trigeminal Nuclei by the Extrinsic Protractor Muscles

(A–D) Injection of ΔG -rabies-mCherry in the tip of the snout (A) leads to retrograde labeling in the lateral most part of the facial nucleus (B) and transsynaptic labeling in the parafacial region (C) and the pre-Bötzing complex (D). Note the absence of labeled cells in the oralis (SpVO) and interpolaris (SpVIr) divisions of the spinal trigeminal sensory complex. Abbreviations are as follows: Amb, ambiguous nucleus; FN, facial nucleus; PF, parafacial region; and pBötC, preBötzing complex. Lowercase letters in (A) indicate the corresponding vibrissa rows.

Assessment of Reflex Latency

The latency of a reflex is the sum of the time delay for motoneuron activation after stimulus onset plus the time delay for muscle contraction after motoneuron firing. From the above intracellular recordings, motoneurons were activated or inhibited about 3.5 ms after stimulus onset. To measure the latency of vibrissa motion induced by the spiking of motoneurons, vibrissae were observed under a stereomicroscope to detect movements induced by cell firing

elicited by the firing of action potentials during intracellular current injection (20 cells). Otherwise, motoneurons were considered as extrinsic motoneurons, which included motoneurons whose firing led to the retraction of two to six vibrissae (four cells) and motoneurons that displayed respiratory modulation (three cells). The other motoneurons remained uncharacterized (five cells).

In ketamine and xylazine-anesthetized rats, facial motoneurons had no spontaneous activity, and air-puff deflection of the vibrissae did not elicit extracellular spiking activity. When cells were recorded intracellularly, we observed a short-latency hyperpolarization in all intrinsic motoneurons (20 cells) upon deflection of the vibrissae (Figure 3A), irrespective of whether air puffs deflected the vibrissa driven by the cell or the adjacent vibrissae. Air puffs directed toward the tip of the nose did not elicit any response. The hyperpolarization had a mean onset latency of 3.5 ± 0.4 ms, and it was often followed by depolarizing events that occasionally led to spike discharge (Figure 3B, arrows). The hyperpolarization reversed polarity at about -70 mV (Figure 3C), and it became rapidly depolarizing, i.e., within 1 min, after impalement with a KCl-filled pipette (five cells; Figure 3D). Thus, this early event was identified as a chloride-mediated inhibitory postsynaptic potential (IPSP).

In pad retractor motoneurons (four cells), deflection of a vibrissa induced a depolarization at a mean latency of 3.3 ± 0.2 ms (four cells; Figure 3E); no response was observed in the other motoneurons (eight cells). The data of Figure 3F illustrate the time course of vibrissa-evoked responses in facial motoneurons together with the local field potential recorded in subnucleus SpVO. One can appreciate the fast onset of motoneuronal responses, which lagged the onset of the field potential by a mere 0.5 ms.

driven by current injection. Once protraction of a single vibrissa was detected, a piezoelectric film was placed in contact with the rostral edge of the vibrissa. This allowed an accurate measurement of the time delay between the firing of an action potential and the initiation of vibrissa protraction (Figures 3G and 3H). The mean latency of protractions was 7.5 ± 0.4 ms (ten cells; 1,293 spikes), which is within the range of latencies, i.e., 7.6 ± 2.5 ms, reported by video tracking (Herfst and Brecht, 2008). Together these results indicate that the shortest reflex latency in the vibrissa-trigemino-facial loop is in the range of 11–13 ms, which is in accord with the reflex latency of 13 ms estimated for freely exploring rats (Mitchinson et al., 2007).

Anatomical Substrate for Reflex Excitation and Inhibition in Rats

The short latency of vibrissa-evoked responses in facial motoneurons indicates that sensory inputs must arise from the trigeminal sensory complex. Transsynaptic labeling studies in mice showed that the subnucleus SpVO contains both glutamatergic and GABAergic or glycinergic premotor neurons that target motoneurons that drive the intrinsic vibrissa muscles. In contrast, subnucleus SpVIr contains a single population of glutamatergic premotor neurons that target motoneurons that drive the extrinsic retractor muscles (Takato et al., 2013; Sreenivasan et al., 2015). We thus investigated the origin of the trigemino-facial excitatory and inhibitory inputs that target the intrinsic and pad retractor motoneurons in rats. Fluorogold was injected iontophoretically in the ventral lateral facial nucleus, and parasagittal sections of the trigeminal sensory nuclei were processed for in situ hybridization using a vesicular GABA transporter (VGAT) probe. Three injections were restricted to the ventral lateral part of the facial nucleus (Figure 4A), with no spread of

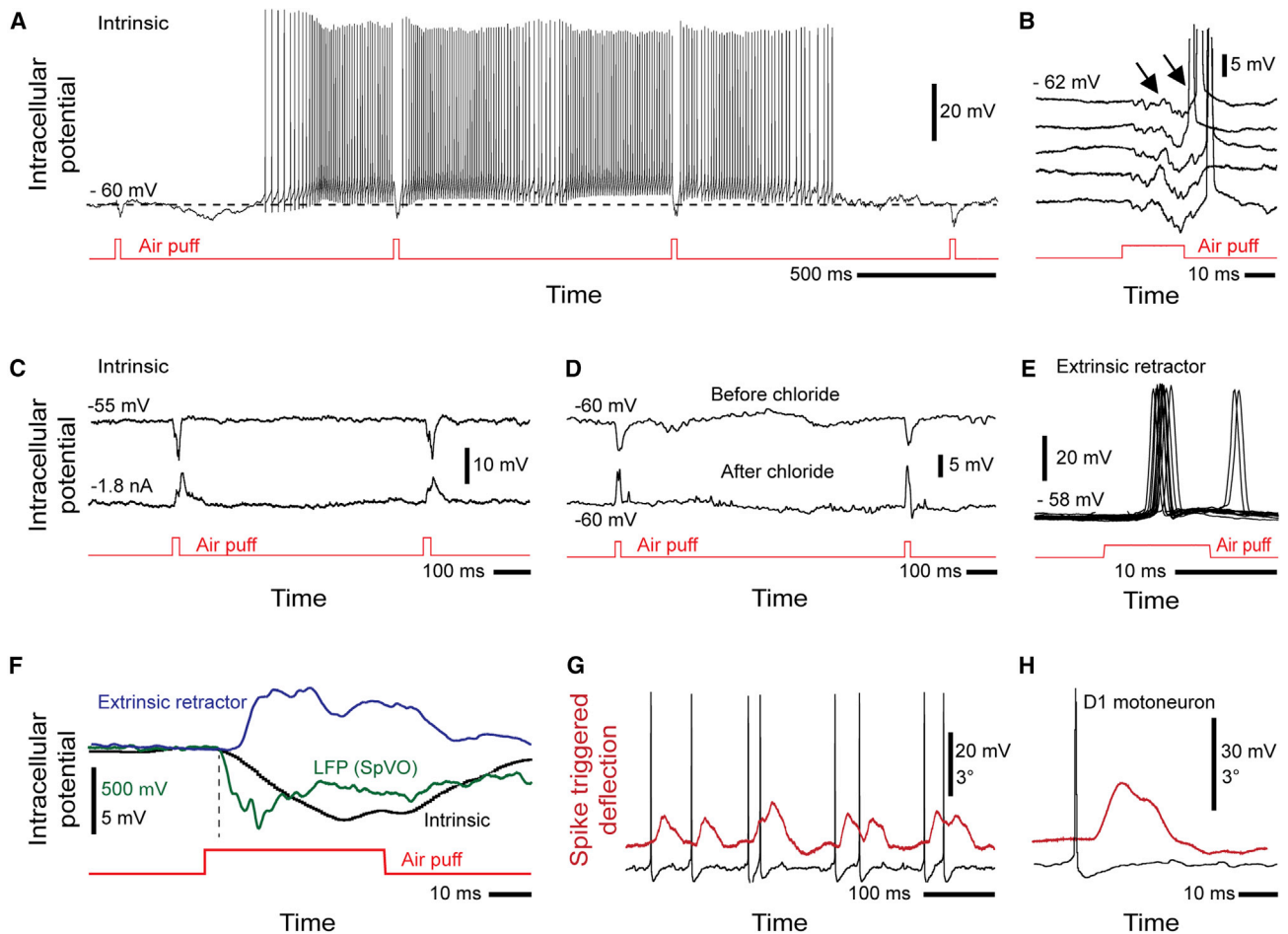


Figure 3. Intracellular Evidence for Sensory Feedback in Facial Motoneurons following Deflection of the Vibrissae

(A) In intrinsic motoneurons, vibrissa deflection induces a short-latency hyperpolarization at an average latency of 3.5 ± 0.4 ms. A transient small depolarizing current was injected to induce cell firing.

(B) In some intrinsic motoneurons, the early hyperpolarization was interrupted or followed by depolarizing events that triggered an action potential (arrows; action potentials are cropped).

(C and D) In intrinsic motoneurons, the hyperpolarization triggered by air puff deflection of the vibrissae reversed in sign upon hyperpolarizing current injection (C), and it became depolarizing shortly after cell impalement with a KCl-filled pipette (D).

(E) In pad retractor motoneurons, passive vibrissa deflection induces a prompt excitation. The ten superimposed traces in this panel are from a motoneuron that drove retraction of vibrissae E1, E2, E3, D1, D2, and D3.

(F) The time course of sensory-evoked responses in an intrinsic motoneuron and a pad retractor motoneuron with that of the local field potential (LFP) recorded in the subnucleus SpVO. Each trace is the average of 35 responses. Note the very short delay, about 0.5 ms, between the onset of the LFP (dashed line) and the onset of intracellular events.

(G) Traces show how the latency of protraction after a motoneuronal spike was measured. In this example, spikes were triggered by current injection in a D1 motoneuron, and a piezoelectric film was used to monitor displacement of vibrissa D1 (red trace).

(H) Spike-triggered average protraction of vibrissa D1 (34 events).

the tracer in the dorsolateral sector where retractor muscles are represented. In these three cases, we found retrogradely labeled cells nearly exclusively in the oralis nucleus (Figure 4A), where 24% (159 of 652) of labeled cells expressed the VGAT transcript (Figure 4B). Assuming that oralis neurons are glutamatergic or GABAergic or glycinergic (Ge et al., 2014; Avendaño et al., 2005; Takatoh et al., 2013), one can infer that oralis premotor neurons provide both glutamatergic and GABAergic or glycinergic inputs to motoneurons that drive the intrinsic vibrissa muscles.

It was previously reported that trigeminal premotor neurons that drive the extrinsic retractor motoneurons preferentially cluster in the SpVlr (Sreenivasan et al., 2015). We thus examined whether interparalis cells that project to the facial nucleus also project to the posterior group (Po) of the thalamus. We used a conditional labeling strategy, which consists of injecting a retrograde lentivirus that expresses Cre in the Po thalamus (RG-LV-hSyn-Cre) and an adeno-associated virus (AAV) Flex-eGFP vector in the SpVlr (Figures 4C–4E). This approach revealed a collateral projection to the facial nucleus from interparalis cells

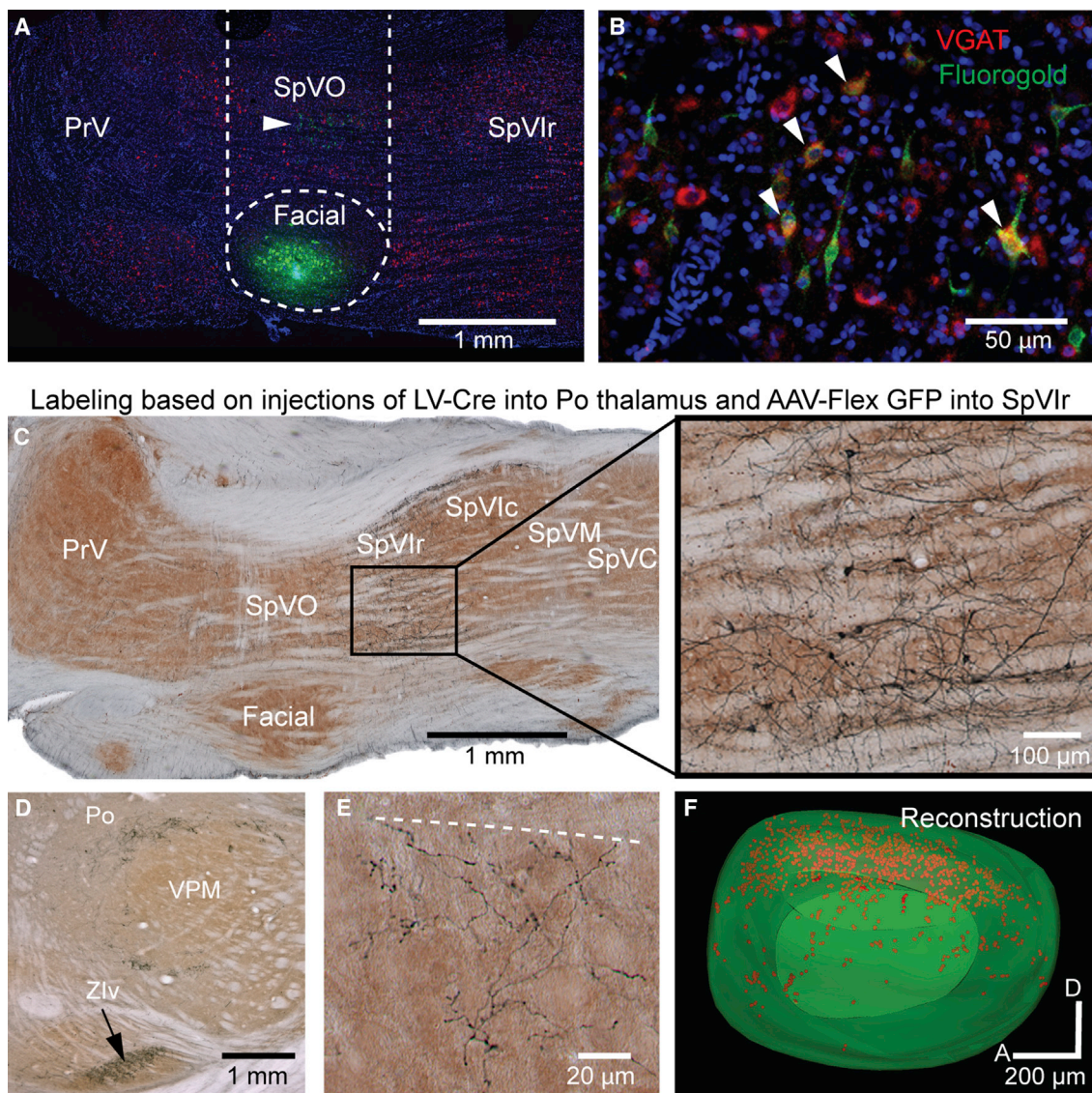


Figure 4. Anatomical Substrate for the Trigemino-Facial Reflex

(A and B) Fluorogold was injected in the ventral lateral facial nucleus. The arrowhead indicates the location of a cluster of retrogradely labeled cells in subnucleus SpVO; the dashed lines delineate subnucleus SpVO (A). In situ hybridization was used to label subnucleus SpVO neurons that express VGAT (arrowheads in B). (C–F) Interpolaris neurons that project to the Po thalamus were selectively labeled by injecting RG-LV-hSyn-Cre into the Po thalamus and AAV-Flex GFP into the subnucleus SpVlr. The framed area in (C) is enlarged in (D). Anterograde labeling of interpolaris axons reveals terminal fields in the Po thalamus and the ventral part of zona incerta (D), as well as in the dorsal lateral division of the facial nucleus (E). The dashed line in (E) indicates the dorsal border of the facial nucleus. The preferential distribution of subnucleus SpVlr terminals in the dorsal lateral sector of the facial nucleus is illustrated in the 3D map in (F) (a, anterior; d, dorsal). Sagittal sections (C–F) were counterstained for cytochrome oxidase. Abbreviations are as follows: PrV, principal trigeminal nucleus; SpVO, oralis subnucleus of the spinal trigeminal complex; SpVlr, rostral division of the interpolaris subnucleus of the spinal trigeminal complex; SpVlc, caudal division of the interpolaris subnucleus of the spinal trigeminal complex; SpVM, muralis sector of the spinal trigeminal complex; SpVC, caudal subnucleus of the spinal trigeminal complex; and Zlv, ventral division of zona incerta.

that projected to the Po thalamus (Figure 4F). The three-dimensional map of Figure 4G shows that the vast majority of labeled terminals were located in the dorsal lateral sector of the nucleus, where pad retractor motoneurons are clustered. This result is direct evidence that reflex activation of pad retractor motoneurons is mediated, at least in part, by glutamatergic interpolaris cells that project to the Po thalamus.

Anatomical Substrate for Trigemino-Facial Reflex in Mice

A prior study in mice revealed that subnucleus SpVO provides both glutamatergic and GABAergic or glycinergic inputs to the intrinsic protractor motoneurons, while glutamatergic SpVlr neurons innervate the extrinsic retractor motoneurons (Takato et al., 2013). We thus examined whether interpolaris cells that

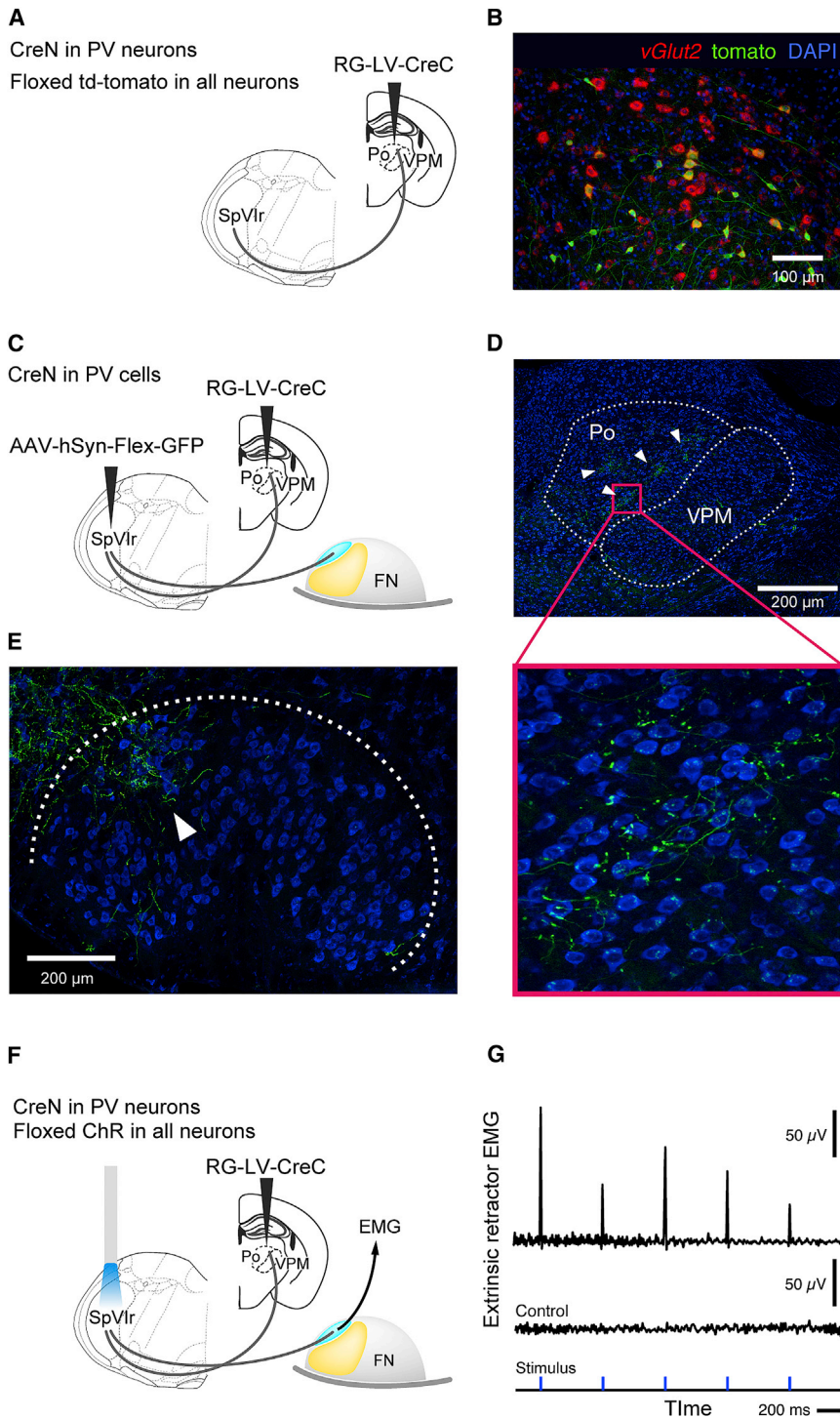


Figure 5. Characterization of Subnucleus SpVlr Neurons that Project to the Po Thalamus and Are Involved in the Trigemino-Facial Reflex

These data make use of a split-Cre strategy (Wang et al., 2012; Stanek et al., 2016). The starting substrate in all cases is mice that are engineered to express CreN in neurons that naturally express parvalbumin. Retrograde lentivirus pseudotyped with FuGB2-coat that encodes CreC (RG-LV-CreC) was injected into the Po thalamus. Thus, functional Cre is reconstituted in parvalbumin (Pv)-positive neurons that project to the Po thalamus.

(A) Schematic of experiment to confirm that Pv neurons in subnucleus SpVlr that further project to the Po thalamus will form excitatory synapses. Pv-CreN mice were crossed to tdTomato reporter mice so that all neurons contain the Cre-dependent tdTomato (Pv-CreN;Ai14). Here the functional Cre leads to expression of tdTomato in Pv-positive neurons that project to the Po thalamus. (B) In situ hybridization performed on mice prepared as in (A) shows that vGlut2 (pseudo-colored red) is co-expressed in neurons that stain positive for tdTomato (anti-RFP pseudo-colored green) (coronal section, counter-staining with DAPI).

(C) Schematic of experiment to confirm that Pv neurons in subnucleus SpVlr that further project to the Po thalamus also project to the facial motor nucleus. AAV that encodes Cre-dependent GFP (AAV-hSyn-Flex-GFP) was injected into subnucleus SpVlr at the same time that RG-LV-CreC was injected into the Po thalamus in Pv-CreN mice. Only Pv-positive SpVlr neurons that project to the Po thalamus will express GFP, and the axonal collaterals of labeled neurons in the FN can be visualized.

(D) Low- and high-magnification views of terminals (green) in the Po thalamus for mice prepared as in (C). Arrows point to labeled terminals (coronal section, counter staining with NeuroTrace blue).

(E) Terminals (green) in the FN for mice prepared as in (C). Coronal section shows the region where extrinsic motoneurons are located and counter staining with NeuroTrace blue are shown.

(F) Schematic of experiment to confirm that Pv neurons in the SpVlr that further project to the Po thalamus can drive motoneurons for the extrinsic muscles in the mystacial pad (Figure 1B). Pv-CreN mice were crossed to channelrhodopsin (ChR2) reporter mice so that all neurons contain Cre-dependent (Pv-CreN;Ai320). Here the functional Cre leads to the expression of ChR2 in Pv-positive neurons that project to the Po thalamus. A cannula for an optical fiber was implanted into the subnucleus SpVlr, and electromyogram (EMG) electrodes were implanted in the extrinsic muscles (Berg and Kleinfeld 2003).

(G) Data from mice, lightly anesthetized with ketamine and xylazine, prepared as in (F). Light pulses at 440 nm, 20 ms wide, were delivered at 500-ms intervals. The ChR2 mice showed retractor muscle activation upon light stimulation, while control animals (without RG-LV-CreC injection) did not show any responses to the light stimulation.

innervate pad retractor motoneurons also project to the Po thalamus in mice. Motivated by a past study (Chiaia et al., 1992), we found that parvalbumin (Pv) is expressed in excitatory (glutama-

tergic) SpVlr neurons. To determine whether Pv+ SpVlr cells represent the premotor neurons that project to both the Po thalamus and extrinsic facial motoneurons, we employed a split-Cre

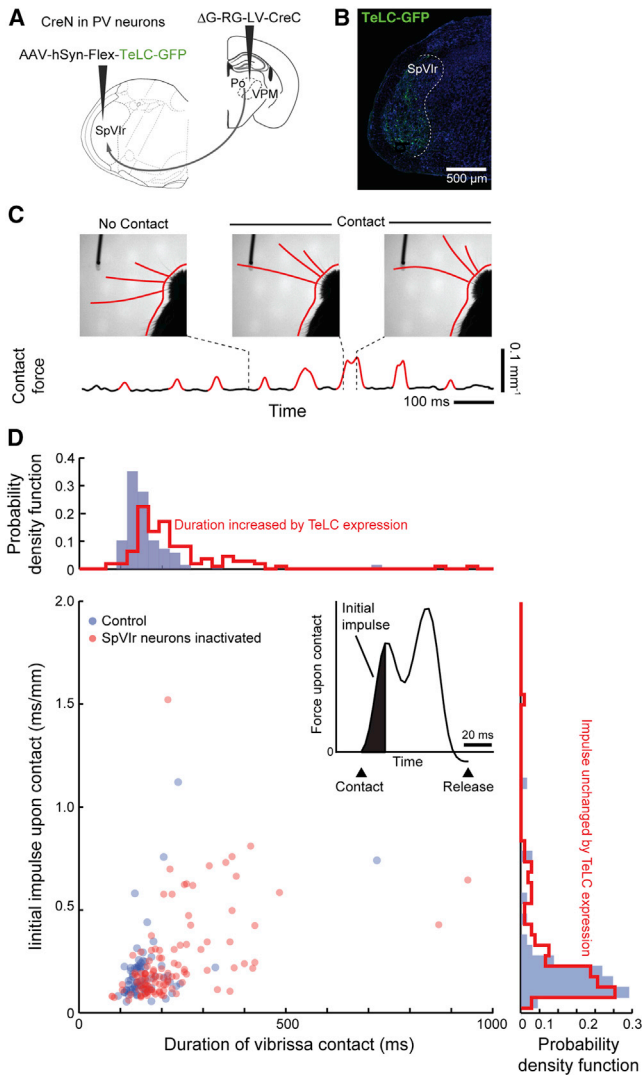


Figure 6. Silencing of Subnucleus SpVlr Neurons that Project to the Po Thalamus Alters the Trigemino-Facial Reflex

(A) Schematic of experiment. RG-LV-CreC is injected into the Po thalamus in Pv-CreN mice so that functional Cre is reconstituted in Pv-positive neurons that project to the Po thalamus. Concurrent with the RG-LV-CreC injections, AAV that encodes Cre-dependent expression of tetanus toxin light chain (TeLC) linked to GFP (AAV-hSyn-Flex-TeLC-GFP) was injected into the subnucleus SpVlr. Thus, only Pv-positive SpVlr neurons that project to both the Po thalamus, as well as send collaterals to the FN, will have their transmission silenced by tetanus toxin.

(B) Post hoc histology shows expression of TeLC-GFP (pseudo-colored green) in SpVlr cells (coronal section, counter staining with NeuroTrace blue).

(C) Changes in the curvature, k , of the vibrissa upon contact with an edge (red). Contact force is proportional to the curvature. At high forces a transient drop, or dip, occurs (see also Figure 1A).

(D) Scatterplot of the impulse upon contact versus the width of the contact interval for contact on the intact side versus the side with feedback to the extrinsic retractor muscle, i.e., Pv-positive SpVlr neurons that project to both the Po thalamus and to the extrinsic facial motoneurons, silenced. The impulse is computed as the curvature, which serves as a surrogate for the force at the base of the vibrissa, integrated over the onset of the contact (inset), i.e., $\text{Impulse} = \int_0^{\text{First peak}} \kappa(t) dt$. The interval is taken as the full period of contact. The computed impulse is the same for intact and silenced sides, as shown by

system (Wang et al., 2012; Stanek et al., 2016). Specifically, we generated Pv-CreN knockin mice, and we injected retrograde lentivirus that expresses CreC (RG-LV-CreC) in the Po in Pv-CreN;Ai14 (Cre-dependent tdTomato reporter) double-transgenic mice. In this way, Pv+ SpVlr cells projecting to the Po were labeled with tdTomato.

In situ hybridization (three mice) demonstrated that the vast majority ($97\% \pm 1\%$) of tdTomato-labeled neurons were vGlut2 positive (Figures 5A and 5B). We next injected RG-LV-CreC into the Po thalamus of Pv-CreN mice (four mice; Figure 5C), and AAV-encoding Cre-dependent GFP was injected into the SpVlr. This approach ensures that only Pv-positive SpVlr neurons projecting to the Po thalamus are labeled in each mouse. We found that, just like in rats, GFP-labeled SpVlr neurons that projected to the Po thalamus gave off collaterals to the dorsolateral sector of the facial motor nucleus (Figures 5D and 5E). Optogenetic stimulation of Po-projecting SpVlr neurons that expressed channelrhodopsin further confirmed that the SpVlr-Po-facial dual projection activates muscle nasolabialis (six mice; Figures 5F and 5G).

Silencing SpVlr Premotor Neurons Prolongs Vibrissa Contact Time

Lastly, we examined whether silencing the SpVlr-facial projection affects the kinematics of whisking upon vibrissa contact in naive, head-restrained mice. This projection was inactivated unilaterally by injecting RG-LV-CreC into the Po thalamus of Pv-CreN animals and AAV encoding Cre-dependent TeLC-GFP into the SpVlr (six mice; Figures 6A and 6B). Contact-induced transient vibrissa reaction was assessed by a change in vibrissa curvature (Figure 6C). In the naive mice used for this manipulation, retraction was observed in 3% and 7% of the cases on the normal and silenced side, respectively. The profound effect of silencing the SpVlr-facial projection was to significantly prolong contact on the silenced side (Figure 6D; see marginal on top), consistent with a lack of involvement of active retraction through the extrinsic retractor muscles (Figure 1B). On the other hand, and consistent with the absence of retractor muscle activity at the onset of protraction, the mechanical impulse (Figure 6D; inset) applied during the initial phase of contact remained unaffected by silencing the SpVlr-facial projection (Figure 6D; see marginal on right).

DISCUSSION

We have completed the wiring diagram of the shortest sensorimotor loops for reflex motion of the vibrissae upon contact with an object (Figure 7). Primary vibrissa afferents excite GABAergic or glycinergic oralis neurons as well as glutamatergic cells in the oralis and interpolaris subnuclei. In turn, both excitatory and inhibitory oralis cells project to the motoneurons for intrinsic muscles, and they activate or suppress, respectively, motoneuron output for the intrinsic muscles that drive vibrissae protraction (Figures 3 and 4). In contrast, Po-projecting

the marginal (right side; $p > 0.1$, two-tailed Kolmogorov-Smirnov [KS] test), but the widths are different (top; $p < 10^{-6}$, two-tailed KS test).

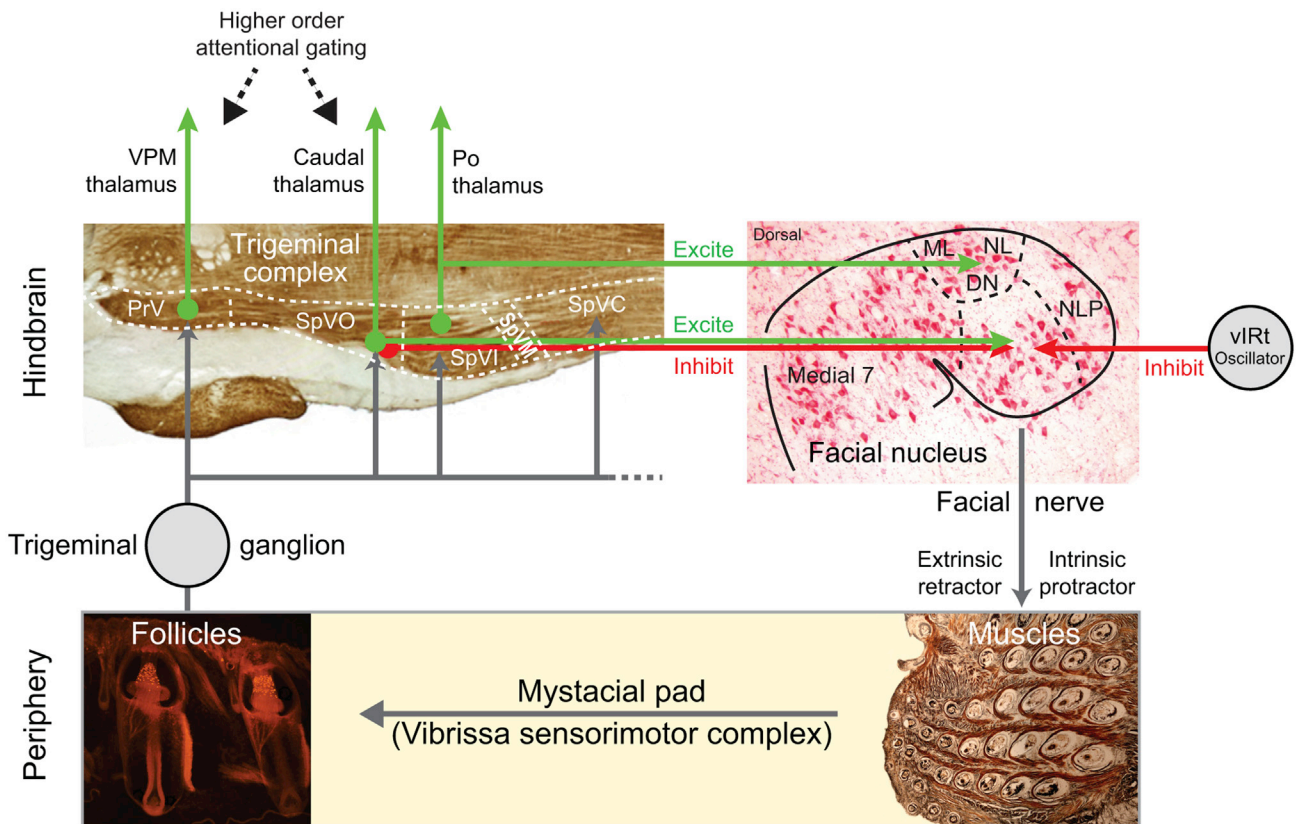


Figure 7. Schematic Diagram of First-Order Feedback Loops Involved in Reflex Motion of the Vibrissae

Intrinsic motoneurons in the ventral lateral sector of the facial nucleus receive both excitatory and inhibitory inputs from the subnucleus SpVO, whereas nasolabialis and maxillolabialis motoneurons in the dorsal lateral sector receive excitatory input from the subnucleus SpVIr neurons that also project to the Po thalamus. Abbreviations are as follows: principal trigeminal nucleus, PrV; spinal trigeminal subnuclei oralis, SpVO; spinal trigeminal subnuclei interopolaris, SpVI; spinal trigeminal subnuclei muralis, SpVM; and spinal trigeminal subnuclei caudalis, SpVC. Muscles nasolabialis (NL) and maxillolabialis (ML) retract the pad, muscle nasolabialis profundus (NLP) protracts the pad, and muscle deflector nasi (DN) deflects the nose.

interopolaris cells excite the motoneurons for extrinsic retractors by means of axon collaterals (Figures 3, 4, 5, and 6). Thus, there are two pathways that can account for fast vibrissa retraction induced by vibrissa contact in prior behavioral studies (Mitchinson et al., 2007; Deutsch et al., 2012), i.e., inhibition of the intrinsic motoneurons and excitation of the extrinsic retractor motoneurons. In contrast to the case for retraction, only one pathway can account for reflexive protraction reported by Nguyen and Kleinfeld (2005) and the touch-induced pumps by Deutsch et al. (2012). In toto, these pathways allow both kinds of reflexes at the appropriate latencies, and their architecture facilitates top-down control of their execution and gain.

Nguyen and Kleinfeld (2005) found exclusively short-latency reflexive excitation of intrinsic and/or nasolabialis motoneurons after stimulation of primary trigeminal afferents. Data were obtained from recording in horizontal brainstem slices in young rats and from electromyographic data in anesthetized adult animals. Two factors likely explain why vibrissa-evoked inhibition of intrinsic motoneurons, or related muscular suppression, was unnoticed in this earlier study. First, the effect of inhibition of the intrinsic motoneurons cannot be detected with electromyographic recordings in anesthetized animals because motoneu-

rons that innervate the intrinsic muscles are already silent. Second, retrograde labeling shows that the inhibitory input to intrinsic motoneurons arises from oralis cells located dorsally relative to the depth of the facial nucleus. Thus, in horizontal slices that include the facial nucleus, most of the inhibitory trigemino-facial connections were likely severed, leaving only the excitatory response. Other studies have addressed feedback connectivity from the trigemino-facial connections in the adult rodent. Sreenivasan et al. (2015) identified a pathway that corresponds to neurons in the subnucleus SpVIr that project to the Po thalamus and the extrinsic muscles (Figure 7). Further, a projection from the muralis division of the trigeminal sensory complex to the facial nucleus has been reported (Matthews et al., 2015). This projection was proposed to be part of a reflex pathway. However, recent anatomical data (Tonomura et al., 2015) and ongoing electrophysiological experiments (Callado-Pérez, A., et al., 2016, Soc. Neurosci., abstract) do not support vibrissa touch signals as afferent input to muralis neurons.

Context Dependence of the Trigemino-Facial Reflex

Inhibitory and excitatory postsynaptic potentials evoked in intrinsic motoneurons by air-puff vibrissa deflection occurred

at nearly the same latency. Yet the dominant effect was inhibition (Figure 3B). As suggested by the rapid reversal of IPSPs after impalement with a chloride-containing pipette and recalling that dendrites of facial motoneurons are electrotonically long (Nguyen et al., 2004), the proximal location of inhibitory synapses likely explains the shunting of more distally located excitatory inputs. A critical issue, though, is the behavioral conditions under which inhibition or excitation prevails. Passive vibrissa deflection produced by an air puff is a useful means to uncover sensorimotor feedback loops involved in reflex control of facial motoneurons. However, this approach does not actually mimic the dynamics of reflex pathways engaged upon vibrissa contact during exploratory behaviors. Given the disynaptic nature of the reflex, its gain is likely modulated by motor strategies and the context of exploration, such as whether exploration occurs in a familiar versus unknown environment (Gordon et al., 2014). It was reported that, when the vibrissae touch a non-attended surface, they show more pronounced bending, suggesting that contact-induced vibrissa is related in some way to the current goals and focus of the animal (Mitchinson et al., 2007; Voigts et al., 2015). Further, reflex retraction is reported to occur only for a quarter of the epochs when the vibrissae contact an object in the head-restrained rat (Deutsch et al., 2012). Yet, the probability of reflexive motion more than doubled when the rats intended to explore an object (Sherman et al., 2017).

How can high-level input control a low-level, disynaptic vibrissa reflex? It is worth reminding that trigeminal sensory nuclei are replete with inhibitory circuits that operate at both the pre- and postsynaptic levels (Ide and Killackey, 1985; Bae et al., 2000, 2005; Furuta et al., 2008). These circuits can be modulated by top-down pathways as well as by cholinergic, serotonergic, and noradrenergic modulatory systems (reviewed in Bosman et al., 2011). Just like in the spinal cord, where both presynaptic and postsynaptic inhibition gates cutaneous inputs during locomotion (Roussigne et al., 2006), similar mechanisms might control the gain and sign of reflex actions for all orofacial pathways mediated by trigeminal neurons that project to the facial nucleus. In particular, the results of modeling efforts (Sherman et al., 2013) imply that high-level feedback may change the relative contribution of intrinsic versus extrinsic muscles in the control of the pump-like motion of retraction followed by protraction upon touch.

STAR★METHODS

Detailed methods are provided in the online version of this paper and include the following:

- KEY RESOURCES TABLE
- CONTACT FOR REAGENT AND RESOURCE SHARING
- EXPERIMENTAL MODEL AND SUBJECT DETAILS
 - Subjects
 - Viruses
- METHOD DETAILS
 - Recording of facial motoneurons
 - Retrograde labeling
 - Virus injection for intersectional labeling
 - Two-color in situ hybridization and immunofluorescence

- Electromyogram and optogenetic activation
- Whisking-based touch
- Vibrissa tracking

AUTHOR CONTRIBUTIONS

M. Deschênes, D.K., and F.W. planned the experiments and wrote the manuscript. M.-A.B., M. Demers, M. Deschênes, J.L., and J.T. carried out the experiments, and all authors analyzed the data.

ACKNOWLEDGMENTS

We thank Conrad Foo for assistance with MATLAB coding and Ehud Ahissar and David S. Deutsch for making their figures available. This research was supported by grants from the Canadian Institutes of Health Research (MT-5877), the National Institute of Mental Health (MH085499), the National Institute of Neurological Disorders and Stroke (NS058668, NS077986, NS101441, and NS0905905), and the National Science Foundation (EAGER - 2144GA).

Received: November 30, 2016

Revised: May 14, 2017

Accepted: June 27, 2017

Published: July 20, 2017; corrected online: August 2, 2017

REFERENCES

- Ashwell, K.W. (1982). The adult mouse facial nerve nucleus: morphology and musculotopic organization. *J. Anat.* 135, 531–538.
- Avendaño, C., Machín, R., Bermejo, P.E., and Lagares, A. (2005). Neuron numbers in the sensory trigeminal nuclei of the rat: A GABA- and glycine-immunocytochemical and stereological analysis. *J. Comp. Neurol.* 493, 538–553.
- Bae, Y.C., Ihn, H.J., Park, M.J., Ottersen, O.P., Moritani, M., Yoshida, A., and Shigenaga, Y. (2000). Identification of signal substances in synapses made between primary afferents and their associated axon terminals in the rat trigeminal sensory nuclei. *J. Comp. Neurol.* 418, 299–309.
- Bae, Y.C., Ahn, H.J., Park, K.P., Kim, H.N., Paik, S.K., Bae, J.Y., Lee, H.W., Kim, K.H., Yoshida, A., Moritani, M., and Shigenaga, Y. (2005). The synaptic microcircuitry associated with primary afferent terminals in the interpolaris and caudalis of trigeminal sensory nuclear complex. *Brain Res.* 1060, 118–125.
- Berg, R.W., and Kleinfeld, D. (2003). Rhythmic whisking by rat: retraction as well as protraction of the vibrissae is under active muscular control. *J. Neurophysiol.* 89, 104–117.
- Bosman, L.W., Houweling, A.R., Owens, C.B., Tanke, N., Shevchouk, O.T., Rahmati, N., Teunissen, W.H., Ju, C., Gong, W., Koekoek, S.K., and De Zeeuw, C.I. (2011). Anatomical pathways involved in generating and sensing rhythmic whisker movements. *Front. Integr. Neurosci.* 5, 53.
- Chiaia, N.L., Bennett-Clarke, C.A., and Rhoades, R.W. (1992). Differential effects of peripheral damage on vibrissa-related patterns in trigeminal nucleus principalis, subnucleus interpolaris, and subnucleus caudalis. *Neuroscience* 49, 141–156.
- Clack, N.G., O'Connor, D.H., Huber, D., Petreanu, L., Hires, A., Peron, S., Svoboda, K., and Myers, E.W. (2012). Automated tracking of whiskers in videos of head fixed rodents. *PLoS Comput. Biol.* 8, e1002591.
- Deschênes, M., Takatoh, J., Kurnikova, A., Moore, J.D., Demers, M., Elbaz, M., Furuta, T., Wang, F., and Kleinfeld, D. (2016). Inhibition, not excitation, drives rhythmic whisking. *Neuron* 90, 374–387.
- Deutsch, D., Pietr, M., Knutsen, P.M., Ahissar, E., and Schneidman, E. (2012). Fast feedback in active sensing: touch-induced changes to whisker-object interaction. *PLoS ONE* 7, e44272.

- Friauf, E. (1986). Morphology of motoneurons in different subdivisions of the rat facial nucleus stained intracellularly with horseradish peroxidase. *J. Comp. Neurol.* 253, 231–241.
- Furuta, T., Timofeeva, E., Nakamura, K., Okamoto-Furuta, K., Togo, M., Kaneko, T., and Deschênes, M. (2008). Inhibitory gating of vibrissal inputs in the brainstem. *J. Neurosci.* 28, 1789–1797.
- Furutani, R., Izawa, T., and Sugita, S. (2004). Distribution of facial motoneurons innervating the common facial muscles of the rabbit and rat. *Okajimas Folia Anat. Jpn.* 81, 101–108.
- Gao, P., Hattox, A.M., Jones, L.M., Keller, A., and Zeigler, H.P. (2003). Whisker motor cortex ablation and whisker movement patterns. *Somatosens. Mot. Res.* 20, 191–198.
- Ge, S.N., Li, Z.H., Tang, J., Ma, Y., Hioki, H., Zhang, T., Lu, Y.C., Zhang, F.X., Mizuno, N., Kaneko, T., et al. (2014). Differential expression of VGLUT1 or VGLUT2 in the trigeminothalamic or trigeminocerebellar projection neurons in the rat. *Brain Struct. Funct.* 219, 211–229.
- Gordon, G., Fonio, E., and Ahissar, E. (2014). Emergent exploration via novelty management. *J. Neurosci.* 34, 12646–12661.
- Grant, R.A., Mitchinson, B., Fox, C.W., and Prescott, T.J. (2009). Active touch sensing in the rat: anticipatory and regulatory control of whisker movements during surface exploration. *J. Neurophysiol.* 101, 862–874.
- Hattox, A.M., Priest, C.A., and Keller, A. (2002). Functional circuitry involved in the regulation of whisker movements. *J. Comp. Neurol.* 442, 266–276.
- Herfst, L.J., and Brecht, M. (2008). Whisker movements evoked by stimulation of single motor neurons in the facial nucleus of the rat. *J. Neurophysiol.* 99, 2821–2832.
- Hill, D.N., Bermejo, R., Zeigler, H.P., and Kleinfeld, D. (2008). Biomechanics of the vibrissa motor plant in rat: rhythmic whisking consists of triphasic neuromuscular activity. *J. Neurosci.* 28, 3438–3455.
- Hinrichsen, C.F., and Watson, C.D. (1984). The facial nucleus of the rat: representation of facial muscles revealed by retrograde transport of horseradish peroxidase. *Anat. Rec.* 209, 407–415.
- Hires, S.A., Pammer, L., Svoboda, K., and Golomb, D. (2013). Tapered whiskers are required for active tactile sensation. *eLife* 2, e01350.
- Ide, L.S., and Killackey, H.P. (1985). Fine structural survey of the rat's brainstem sensory trigeminal complex. *J. Comp. Neurol.* 235, 145–168.
- Klein, B.G., and Rhoades, R.W. (1985). Representation of whisker follicle intrinsic musculature in the facial motor nucleus of the rat. *J. Comp. Neurol.* 232, 55–69.
- Komiyama, M., Shibata, H., and Suzuki, T. (1984). Somatotopic representation of facial muscles within the facial nucleus of the mouse. A study using the retrograde horseradish peroxidase and cell degeneration techniques. *Brain Behav. Evol.* 24, 144–151.
- Liang, F., Hatanaka, Y., Saito, H., Yamamori, T., and Hashikawa, T. (2000). Differential expression of gamma-aminobutyric acid type B receptor-1a and -1b mRNA variants in GABA and non-GABAergic neurons of the rat brain. *J. Comp. Neurol.* 416, 475–495.
- Matthews, D.W., Deschênes, M., Furuta, T., Moore, J.D., Wang, F., Karten, H.J., and Kleinfeld, D. (2015). Feedback in the brainstem: an excitatory disynaptic pathway for control of whisking. *J. Comp. Neurol.* 523, 921–942.
- Mitchinson, B., Martin, C.J., Grant, R.A., and Prescott, T.J. (2007). Feedback control in active sensing: rat exploratory whisking is modulated by environmental contact. *Proc. Biol. Sci.* 274, 1035–1041.
- Moore, J.D., Deschênes, M., Furuta, T., Huber, D., Smear, M.C., Demers, M., and Kleinfeld, D. (2013). Hierarchy of orofacial rhythms revealed through whisking and breathing. *Nature* 497, 205–210.
- Moore, J.D., Mercer Lindsay, N., Deschênes, M., and Kleinfeld, D. (2015). Vibrissa self-motion and touch are reliably encoded along the same somatosensory pathway from brainstem through thalamus. *PLoS Biol.* 13, e1002253.
- Nguyen, Q.T., and Kleinfeld, D. (2005). Positive feedback in a brainstem tactile sensorimotor loop. *Neuron* 45, 447–457.
- Nguyen, Q.T., Wessel, R., and Kleinfeld, D. (2004). Developmental regulation of active and passive membrane properties in rat vibrissa motoneurons. *J. Physiol.* 556, 203–219.
- Pinganaud, G., Bernat, I., Buisseret, P., and Buisseret-Delmas, C. (1999). Trigeminal projections to hypoglossal and facial motor nuclei in the rat. *J. Comp. Neurol.* 415, 91–104.
- Rossignol, S., Dubuc, R., and Gossard, J.P. (2006). Dynamic sensorimotor interactions in locomotion. *Physiol. Rev.* 86, 89–154.
- Sachdev, R.N., Berg, R.W., Champney, G., Kleinfeld, D., and Ebner, F.F. (2003). Unilateral vibrissa contact: changes in amplitude but not timing of rhythmic whisking. *Somatosens. Mot. Res.* 20, 163–169.
- Sherman, D., Oram, T., Deutsch, D., Gordon, G., Ahissar, E., and Harel, D. (2013). Tactile modulation of whisking via the brainstem loop: statechart modeling and experimental validation. *PLoS ONE* 8, e79831.
- Sherman, D., Oram, T., Harel, D., and Ahissar, E. (2017). Attention robustly gates a closed-loop touch reflex. *Curr. Biol.* 27, 1836–1843.e7.
- Sreenivasan, V., Karmakar, K., Rijli, F.M., and Petersen, C.C. (2015). Parallel pathways from motor and somatosensory cortex for controlling whisker movements in mice. *Eur. J. Neurosci.* 41, 354–367.
- Stanek, E., 4th, Rodriguez, E., Zhao, S., Han, B.X., and Wang, F. (2016). Supratrigeminal bilaterally projecting neurons maintain basal tone and enable bilateral phasic activation of jaw-closing muscles. *J. Neurosci.* 36, 7663–7675.
- Takato, J., Nelson, A., Zhou, X., Bolton, M.M., Ehlers, M.D., Arenkiel, B.R., Mooney, R., and Wang, F. (2013). New modules are added to vibrissal premotor circuitry with the emergence of exploratory whisking. *Neuron* 77, 346–360.
- Tonomura, S., Ebara, S., Bagdasarian, K., Uta, D., Ahissar, E., Meir, I., Lampl, I., Kuroda, D., Furuta, T., Furue, H., and Kumamoto, K. (2015). Structure-function correlations of rat trigeminal primary neurons: Emphasis on club-like endings, a vibrissal mechanoreceptor. *Proc. Jpn. Acad. Ser. B Phys. Biol. Sci.* 91, 560–576.
- Voigts, J., Herman, D.H., and Celikel, T. (2015). Tactile object localization by anticipatory whisker motion. *J. Neurophysiol.* 113, 620–632.
- Wang, P., Chen, T., Sakurai, K., Han, B.X., He, Z., Feng, G., and Wang, F. (2012). Intersectional Cre driver lines generated using split-intein mediated split-Cre reconstitution. *Sci. Rep.* 2, 497.
- Watson, C.R., Sakai, S., and Armstrong, W. (1982). Organization of the facial nucleus in the rat. *Brain Behav. Evol.* 20, 19–28.
- Welker, W.I. (1964). Analysis of sniffing of the albino rat. *Behaviour* 22, 223–244.
- Wickersham, I.R., Finke, S., Conzelmann, K.K., and Callaway, E.M. (2007). Retrograde neuronal tracing with a deletion-mutant rabies virus. *Nat. Methods* 4, 47–49.
- Zhang, Y., Zhao, S., Rodriguez, E., Takato, J., Han, B.X., Zhou, X., and Wang, F. (2015). Identifying local and descending inputs for primary sensory neurons. *J. Clin. Invest.* 125, 3782–3794.

STAR★METHODS

KEY RESOURCES TABLE

REAGENT or RESOURCE	SOURCE	IDENTIFIER
Antibodies		
Rabbit polyclonal anti-Fluorogold	Fluorochrome LLC	N/A
Rabbit polyclonal anti-GFP	Novus Biological	Cat# NB600-308; RRID: AB_10003058
Rabbit polyclonal anti-GFP	Abcam	Cat# ab290; RRID: AB_303395
Rabbit polyclonal anti-RFP	Rockland	Cat# 600-401-379; RRID: AB_2209751
Donkey anti-rabbit IgG conjugated to FITC	Jackson ImmunoResearch	Cat# 711-095-152; RRID: AB_2315776
Donkey anti-rabbit IgG conjugated to Alexa Fluor 488	Jackson ImmunoResearch	Cat# 711-545-152; RRID: AB_2313584
Biotinylated Goat anti-rabbit IgG	Vector Labs	Cat# BA-9400; RRID: AB_2336202
Sheep anti-DIG conjugated to AP	Sigma-Aldrich	Cat# 11093274910; RRID: AB_514497
Bacterial and Virus Strains		
RG-LV-Cre	Stanek et al., 2016	N/A
RG-LV-CreC	Stanek et al., 2016	N/A
AAV2/8-hSyn-Flex-TeLC-P2A-GFP	Zhang et al., 2015	N/A
AAV2/8-hSyn-Flex-ChR2-EYFP	UNC Vector Core	N/A
AAV2/1-Flex-eGFP	UPenn Vector Core	N/A
Δ G-Rabies-mCherry	Wickersham et al., 2007	N/A
Chemicals, Peptides, and Recombinant Proteins		
Fluorogold	Fluorochrome LLC	N/A
Vectastain Elite ABC HRP kit	Vector Labs	Cat# PK-6100; RRID: AB_2336819
ImmPACT SG peroxidase kit	Vector Labs	Cat# SK-4700; RRID: AB_2314425
3,3'-Diaminobenzidine	Sigma	Cat# D5637
NeuroTrace 435/455 Blue Fluorescent Stain	ThermoFisher	Cat# N21479
Blocking Reagent	Sigma-Aldrich	Cat# 11096176001
Blocking One	Nacalai USA	Cat# 03953-95
Fast Red TR/Naphthol AS-MX	Sigma-Aldrich	Cat# F4648
Experimental Models: Organisms/Strains		
Rats Long Evans (female and males)	Charles River	N/A
Mouse: Pv-CreN	This paper	N/A
Mouse: Ai14	Jackson Laboratory	RRID: IMSR_JAX:007908
Mouse: Ai32	Jackson Laboratory	RRID: IMSR_JAX:012569
Oligonucleotides		
Primers for amplifying in situ template for vGat: fwd 5'- GGC CACCTCCGTGTCCAACAAGTCC-3' rev 5'- CGCGCG TAATACGACTCACTATAGGGGAATTCGCTGGGCTGCTG CATGTTG-3', underline: T7 binding site	Deschênes et al., 2016	N/A
Primers for amplifying in situ template for vGlut2: fwd 5'-CAA GAAGGTGCGCAAGACGCGTACACC-3' rev 5'- CGCGCG TAATACGACTCACTATAGGGTGCCTCAAGCATTTCACAAA ACACTGC-3' underline: T7 binding site	Takatoh et al., 2013	N/A
Software and Algorithms		
MATLAB v.2014a	Mathworks	RRID: SCR_001622
TissueScope LE	Huron Digital Pathology	N/A
NeuroLucida	MBF Bioscience	RRID: SCR_001775
Janelia Whisker Tracker	Clack et al., 2012	https://www.janelia.org/open-science/whisk-whisker-tracking

CONTACT FOR REAGENT AND RESOURCE SHARING

As Lead Contact, Martin Deschênes is responsible for all reagent and resource requests. Please contact Martin Deschênes at martin.deschenes@crulrg.ulaval.ca with requests and inquiries.

EXPERIMENTAL MODEL AND SUBJECT DETAILS

Subjects

Experiments were carried out in 22 Long Evans female rats (250–350 g in mass), and in 5~8 weeks old adult mice (both male and female) according to the National Institutes of Health Guidelines.

Pv-CreN knock-in mice were generated by inserting a 2A sequence, CreN-Intein-N (Wang et al., 2012) and Frt-flanked PGK-neomycin resistance cassette immediately in front of the stop codon of parvalbumin coding sequence by homologous recombination. ES clones with appropriate homologous recombination were selected by Southern blotting. After the knock-in mouse line was established, the Frt-flanked PGK-neomycin resistance cassette was removed by crossing with transgenic mice expressing Flpo in all cells (Jackson Laboratory, Stock No: 007844).

The Ai14 reporter line, which carries a Cre-dependent tdTomato cassette (Jackson Laboratory Stock No: 007908), and the Ai32 reporter line, which carries a Cre-dependent ChR2-EYFP cassette (Jackson Laboratory Stock No: 012569), were crossed to generate Pv-CreN;Ai14 and Pv-CreN;Ai32 mice, respectively.

All experiments were approved by the Institutional Animal Care and Use Committee at Duke University, Laval University, and the University of California at San Diego.

Viruses

RG-LV-CreC and RG-LV-Cre were designed and produced as described (Stanek et al., 2016). AAV2/8-hSyn-Flex-TeLC-P2A-GFP was designed and produced as described (Zhang et al., 2015). ΔG-Rabies-mCherry was produced as described (Takato et al., 2013). AAV2/8-hSyn-DIO-GFP (8×10^{12} ifu/ml) was purchased from the University of North Carolina Vector Core. AAV2/1-EF1a-ChR2-EYFP-WPRE (6×10^{12} ifu/ml) was purchased from the University of Pennsylvania Vector Core).

METHOD DETAILS

Recording of facial motoneurons

Rats were anesthetized with ketamine (75 mg/kg) and xylazine (5 mg/kg), and body temperature was maintained at 37.5°C with a thermostatically controlled heating pad. Respiration was monitored with a cantilevered piezoelectric film (LDT1 028K; Measurement Specialties) resting on the rat's abdomen just caudal to the torso. Facial motoneurons were recorded intracellularly with micropipettes (tip diameter, 1 μm) filled with either 0.5 M potassium acetate, or 3 M potassium chloride. Vibrissae were deflected rostralward or caudalward with the use of 10–70 ms air-puffs. The time delay between the command voltage and the onset of vibrissa deflection was measured with a piezoelectric film positioned at the same distance from the puffer tip. A piezoelectric film was used to measure the latency of vibrissa protraction induced by motoneuron spiking. An insect pin was glued to the piezoelectric film and placed in contact with the rostral edge of the vibrissa. Although resonance of the sensor altered the apparent time course of vibrissa retraction, this allowed an accurate measurement of protraction onset. All signals were sampled at 10 kHz and logged on a computer using the Labchart acquisition system (AD Instruments).

Retrograde labeling

To determine the origin and neurotransmitter content of trigemino-facial neurons, we combined retrograde labeling with in situ hybridization in rats. Fluorogold, prepared 1% (w/v) in cacodylate buffer, pH 7.1, was delivered iontophoretically in the ventral lateral facial nucleus using micropipettes (tip diameter, 8 μm) and positive current pulses (250 nA; duration 2 s; half-duty cycle for 15 min).

After a survival of 3 days, rats were perfused with paraformaldehyde, 4% (w/v), and parasagittal sections of the brainstem were cut on a freezing microtome (50 μm thickness) and processed for in situ hybridization using a vesicular GABA transporter (VGAT) probe according to standard protocols (see below). Sections were then immunostained with a rabbit anti-Fluorogold antibody (Fluorochrome LLC), and an anti-rabbit IgG conjugated to Alexa 488 (Jackson ImmunoResearch). Cell counts were made from stacks of confocal images scanned at 20x magnification. As a reference, oralis subnucleus of the spinal trigeminal complex was defined as the region situated between the rostral and caudal edges of the facial nucleus. A slide scanner (TissueScope CF, Huron Technologies) was used to acquire large-scale images that were imported in Neurolucida (MBF Bioscience) to map the location of cells and axonal terminals labeled by virus infection.

Virus injection for intersectional labeling

To label premotor neurons that innervate muscle nasolabialis profundus, we injected Δ G-Rabies-mCherry (1 μ l) in the tip of the snout in five juvenile mice (P2-P6) that expressed the missing G complement in cholinergic neurons (Takatoth et al., 2013). Mice were perfused after a survival period of 5 days.

To determine whether facial premotor neurons in trigeminal nuclei also project to the thalamus we injected a pseudotyped lentivirus expressing CRE recombinase (RG-LV-hSyn-Cre) in the posterior group (Po) of the thalamus (300 nl) and AAV.2/1.hSyn.ChR2.EYFP.WPRE in the rostral part of the nucleus interparietalis (SpVlr) (100 nl). Rats were perfused after a survival of 12 days.

In both of the above cases, parasagittal sections of the brainstem were cut at 50 μ m, immunostained with a rabbit anti-GFP antibody (1:1000; Novus Biological), a biotinylated anti-rabbit IgG (1:200; Vector Labs), the avidin/biotin complex (Vectastain ABC kit; Vector Labs), and the SG peroxidase substrate (Vector Labs). Sections were counterstained for cytochrome oxidase to outline trigeminal sensory nuclei as well as the facial nucleus. Confocal microscopy was employed to count the number of doubly labeled cells in experiments that combined retrograde labeling with in situ hybridization.

For intersectional labeling RG-LV-CreC (800 nl) was injected in Po thalamus of Pv-CreN mice, and AAV-hSyn-Flex-GFP (500 nl) was injected in the SpVlr. Viruses were delivered at 100 nl/min using a glass capillary connected to an UltraMicroPump controlled by a SYS-Micro4 Controller (World Precision Instruments). After a survival of over 3 weeks mice were perfused as above. In situ hybridization was performed as described (Liang et al., 2000; Takatoth et al., 2013) on 40 μ m floating sections that were hybridized with either DIG-labeled vGAT probe or vGlut2 probe. Cell counts were made from stacks of confocal images scanned at 20-x magnification. Immunofluorescence was performed on 80 μ m floating sections that were counter-stained for NeuroTrace (Molecular Probes, N21479). Sections were imaged with a confocal microscope (LSM700; Carl Zeiss).

Two-color in situ hybridization and immunofluorescence

In situ hybridization was performed using protocols based on Liang et al. (2000). First, 50 μ m parasagittal sections (rats) or 40 μ m coronal sections (mice) were permeabilized in phosphate buffered saline (PBS) containing 0.3% Triton X-100 for 20 min, treated with proteinase K (5 μ g/ml in PBS, 30 min, 37°C), and acetylated (10 min at room temperature). Then sections were incubated in a pre-hybridization buffer solution containing 2% Blocking Reagent (Sigma-Aldrich), 0.1 M maleic acid buffer, 0.15 M NaCl, 50% formamide, 0.1% N-lauroylsarcosine (NLS), 0.1% dodecyl sulfate (SDS) and 5x saline-solution citrate (SSC) for 60 min at 60°C. Sections were hybridized with digoxigenin-labeled VGAT or vGlut2 probes overnight at 60°C. Sections were washed in the pre-hybridization buffer and incubated with sheep anti-digoxigenin antibody conjugated to alkaline phosphatase (1:3500; Sigma) and rabbit anti-Fluorogold (1:200; Fluorochrome) or rabbit anti-RFP (1:500, Rockland). Hybridization signals were visualized using Fast Red TR/Naphthol AS-MX (Sigma-Aldrich). Then sections were incubated with a donkey anti-rabbit secondary antibody conjugated to Alexa Fluor 488 (1:1000; Jackson ImmunoResearch) and DAPI. After two washes in buffer solution, sections were mounted on glass slides and imaged with a confocal microscope (LSM700; Carl Zeiss). Cell counts were made from stacks of confocal images scanned at 20x magnification.

Electromyogram and optogenetic activation

Pv-CreN;Ai32 mice were injected with RG-LV-CreC into Po thalamus. After viral injection and optic cannula implantation, EMG electrodes were placed in the nasolabialis muscle as described previously (Berg and Kleinfeld 2003). For optogenetic activation experiments, mice were lightly anesthetized with ketamine and xylazine and held in a custom-made head-fix apparatus. Mice were connected to a blue laser (473 nm, OptoEngine LLC) through a fiber optic (200 μ m core diameter, Thorlabs) with ferrule connector (Thorlabs) that was implanted above the SpVlr and secured with cyanoacrylate and Meta-bond (Parkell). Twenty ms laser pulses were delivered at 500 ms interval.

Whisking-based touch

Pv-CreN mice were injected with RG-LV-CreC and AAV2/8-hSyn-Flex-TeLC-P2A-GFP into Po thalamus and subnucleus SpVlr, respectively. Behavioral experiments were performed 14-21 d after virus injection. Mice were held in a custom-made head-fix apparatus using the pre-attached head plate and the mouse body was positioned into a 3D-printed body tube. Mice were acclimatized to head-fixation in the apparatus. One day before behavioral experiments, mice were anesthetized and all vibrissae except the C row vibrissae were trimmed. During the recording sessions, mice were head-restrained and presented with a vertical pole. All experiments were carried out in the dark under infrared illumination. Spontaneous touch behavior was captured with a high-speed camera (Basler) at 500 fps. Subnucleus SpVlr on the left side was the TeLC-silenced side, and the subnucleus on right side was intact and used as control.

Vibrissa tracking

We tracked the vibrissa curvature across 167 behavioral sessions in which mice contacted the object (77 sessions for the SpVlr-silenced side and 90 sessions for the intact side). Each session contains multiple episodes of object contacts, as well as whisking in air or quiet resting periods. We applied a custom vibrissa tracking algorithm, similar to that in Clack et al. (2012), to measure

the curvature of the vibrissae in the successive video frames. Since tracking gives rise to the sequence of points that represent the vibrissa shape, we can directly calculate the curvature within a plane, denoted κ , at any point along the vibrissa. We use

$$\kappa = \frac{y''}{(1+y'^2)^{\frac{3}{2}}}$$

where $y' = dy/dx$. We calculated the averaged curvature of three points along the contact section, and then corrected the calculation based on the vibrissa's intrinsic curvature. The curvature traces of each clip were then smoothed by a Gaussian kernel of appropriate variation. All data were analyzed using routines written in MATLAB, Mathworks).